3D synchrotron X-ray microtomography for paper structure characterization of *z*-structured paper by introducing micro nanofibrillated cellulose

Charfeddine Mohamed Ali, Bloch Jean-Francis, Boller Elodie, and Mangin Patrice

KEYWORDS: Micro Nano Fibrillated Cellulose, 3D Synchrotron X-ray microtomography, Paper structure, Porosity

SUMMARY: A layer of Micro Nanofibrillated Cellulose (MNFC) was added during the formation of TMP paper to create a *z*-structured paper. A MNFC layer was added either on the top or in the middle of the thickness of a TMP sheet using a Dynamic Sheet Former. The MNFC layer basis weight was varied from 2 to 20 g.m^{-2} for a final paper basis weight of 60 g.m^{-2}. 3D images of the paper structure were obtained by Synchrotron X-ray microtomography, showing that localized MNFC fibrils were retained in the paper structure. The small dimensions of CNF, particularly in width, and the presence of the calcium carbonate in the MNFC layer permit to clearly differentiate the TMP fibers from the MNFC fibrils. The porosity profiles for 100% TMP sheet and 100% MNFC film present a constant internal *bulk* porosity at about 75% and 38%, respectively. Porosity profiles of the *z*-structured paper display the presence of 2 or 3 different porosity zones in the internal *bulk* region. These results confirm the possibility to design papers with targeted porosity gradients in the *z*-direction without paper post treatment.

ADDRESSES OF THE AUTHORS: Charfeddine Mohamed Ali (Mohamed.Ali.Charfeddine@uqtr.ca**)** and **Mangin Patrice (**Patrice.Mangin@uqtr.ca**)**:
Lignocellulosic Materials Research Centre, Pavillon CIPP 3351, boul. des Forges, Trois-Rivières, Qc, Canada, G9A 5H7
Boller Elodie (boller@esrf.fr)**,** European Synchrotron Radiation Facility, 71 Avenue des Martyrs, 38000 Grenoble, France
Bloch Jean-Francis (Jean-Francis.Bloch@pagora.grenoble-inp.fr), Grenoble Institute of Technology - Pagora, 461 rue de la Papeterie - CS 10065 - 38402 Saint Martin d'Hères Cedex, France**,**
Corresponding author: Charfeddine Mohamed Ali

Over the last years, Micro Nanofibrillated Cellulose (MNFC), a cellulose filament with micro dimension in length and nano dimension fibrils in width, has become relatively straightforward to produce both in the laboratory and pilot scale. Accordingly, studies of the benefits of its addition in composites have known a considerable growth (Lavoine et al., 2012). Most of the studies are focused on the mechanical performance of MNFC films and composites (Siró, Plackett, 2010). Nowadays, the use of MNFC in papermaking processes is becoming a renewed research topic (Brodin et al., 2014).

MNFC is essentially added by two methods. The first method consists in mixing MNFC to the pulp before paper formation (Eriksen et al., 2008; González et al., 2012), which results in a significant increase in the mechanical properties of the sheet (up to 21% in the tensile index for an MNFC amount of 4%). In the second method, MNFC is coated on the surface of a wet paper sheet (Syverud, Stenius, 2008) which results in developing barrier properties as indicated by paper air permeability drastically dropping (from 6.5×10^4 nm Pa^{-1} s^{-1} to 360 nm Pa^{-1} s^{-1} with a 8 g.m^{-2} MNFC coating). To understand such air permeability reduction, the paper structure was analyzed by scanning electron microscopy (SEM) (Syverud, Stenius, 2008; Aulin et al., 2010). The authors claim that SEM images revealed the capacity of the MNFC to form a dense and closed network that reduced the paper surface porosity. However, these images did not show how the MNFC coating layer interacted with the base paper. Neither of these two addition methods alone is able to improve both mechanical and barrier properties significantly at the same time (Brodin et al., 2014).

The interaction between different paper components (base paper and coat layer) can be analyzed by internal paper structure assessment by three-dimensional (3D) technics. Synchrotron X-ray microtomography (SµT) has been used to obtain 3D structural information of many porous materials (Thibault et al., 2002; Moore et al., 2004; Pyun et al., 2007). It offers the advantage of showing the internal material structure in a non-destructive, non-disturbing way. Recently, the technique was applied to characterize fibrous material such as paper (Samuelsen et al., 1999; Rolland du Roscoat et al., 2005; Rolland du Roscoat et al., 2012). High-resolution images were used to identify the distribution of various inorganic fillers in the paper structure (Rolland du Roscoat et al., 2012).

Z-structuring is proposed here as a new method to add MNFC into paper and board to improve both its barrier and mechanical properties. The possibility of creating a *z*-structured paper, *i.e.* a paper with a controlled continuous layer structure of different density in the thickness of the sheet was tested in laboratory scale. The principle of *z*-structuring is to add MNFC during the paper formation, here on a Dynamic Sheet Former (DSF), which would result in a dense MNFC layer in chosen different positions of the sheet thickness. The basic hypothesis is that the addition of an MNFC layer during papermaking on the top of a TMP layer, so-called *top position*, would lead to a reduction of the surface porosity. The main difference between the here proposed *z*-structuring in the top position and the more common coating technique lies in the assumed presence of a penetration gradient of MNFC in the TMP layer structure. Binding between the MNFC layer and the TMP layer should be stronger than in surface coating only. Furthermore, with a *z*-structuring approach, the MNFC layer may be added in the middle of the sheet thickness, so-called *middle position*, to reduce the paper porosity locally while enhancing significantly the essential barrier and, to a lesser extent, the mechanical properties of the paper or board.

Questions remained to be answered about the real structure creation of *z*-structured paper as to whether the MNFC actually forms a layer at the target position or if it penetrates the TMP layer. To answer these questions, a 3D structure characterization was required.

To verify our assumption, the paper structure was analyzed by SμT with different amounts of MNFC addition in different positions. A visual analysis of the 3D images conveys a qualitative description of the paper structure, but the 3D images may also be analyzed to provide further paper structure information such as paper porosity profile and/or pore size distribution. This article aims to prove the possibility to elaborate *z*-structured paper with targeted structure. Physical properties resulted from these structures are not on the scope of this publication.

Materials and Methods

Thermo-mechanical pulp

The thermo-mechanical pulp (TMP) was provided by Resolute Forest Products (Abibow Book Cream 51.8 g.m^{-2}). It was a mix of bleached and unbleached dried TMP. The pulp Canadian Standard Freeness (CSF) was 254 ml. For paper making, the pulp was dispersed in hot water (90°C) for 5 min in a laboratory blender at a consistency of 0.2wt%.

Micro Nanofibrillated Cellulose

The MNFC was supplied by Omya International AG. It was obtained from a mix of bleached Eucalyptus pulp with ground calcium carbonate (Hydrocarb 50 – GU, Omya) in the ratio of 80% cellulose and 20% filler, which are combined during the manufacture of the MNFC. The mixture at a consistency of 2.72% was heated to 96°C before being pumped, for a total of three passes, through a pilot scale homogenizer (LPN 500 from GEA Niro Soavi). The pressure drop was fixed at 600 bars. The obtained MNFC has a diameter ranging from 20 nm (nano-part) to 15 μm (micro-part) and a length of up to 1 mm. For papermaking, the MNFC suspension was diluted to a concentration of 0.1 wt% fibrils.

Papermaking

The *z*-structuring approach was proposed as a strategy to engineer, *i.e.* custom-tailor, paper properties. It has been verified on the laboratory scale with model structures manufactured on a DSF. Two positions in depth, namely *top* and *middle* of the sheet, were targeted in order to understand both the effects of the MNFC layer inclusion, and the effects of the boundary layers, *i.e.* how the MNFC layer interacts and binds itself to the TMP fiber network. The basis weight of the MNFC layers was varied from 2 to 20 g.m^{-2}. The total basis weight of the *z*-structured sheets for all sheets was 60 g.m^{-2} indicating no measurable loss of MNFC. A 100% TMP sheet, also at 60 g.m^{-2}, and a 100% MNFC sheet at 40 g.m^{-2} have served as references. After wet formation, the sheets were pressed at 2, 3, and 4 bars between two blotting papers before drying at 105°C for 10 min.

X-ray synchrotron microtomography

X-ray synchrotron microtomography measurements were made in the ID19 beamline of the European Synchrotron Radiation Facility (ESRF). The sample was fixed on the top of a piece of Post-it® (3M, St. Paul MN, USA). The Post-it® was glued on the top of a glass capillary. This set-up was then positioned on a rotating stage and irradiated by the X-ray beam. The transmitted beam was recorded using a high-resolution camera. A detailed description of the experimental set-up can be found in Rolland du Roscoat et al. (2005). The transmitted beam was measured for 2 000 different angular positions over 360°. The pixel size was chosen at 0.65 μm. The sample size was 1.4 × 1.4 × paper thickness mm^3. This size is representative of the paper structure as shown by Rolland du Roscoat et al. (2007).

The sample reconstruction from the radiographs was made using algorithms based on the Lambert-Beer law:

$$I_n(x, y) = I_0 \times exp(-\int \mu(x, y, z)dz) \qquad [1]$$

where I_0 and I_n (x, y) represent the intensity of the beam before and after the transmission through the sample, $\{x, y, z\}$ are the set of sample Cartesian coordinates, and μ is the attenuation coefficient.

Results and discussion

3D images

Examples of SμT results are presented in the following images. In *Fig 1*, presenting the 100% TMP paper structure, large fibers with a diameter of about 57 μm can be seen to be interwoven with fines. Preferential fiber orientation is easily observed from *Fig 1b*. The fibers are oriented preferentially in the simulated machine direction (DSF rotation direction). The MNFC film structure is presented in *Fig 2*. The images show a dense structure with apparent very low porosity – as indicated by the reduced black areas in the cross section – when compared with the 100% TMP sheet. As expected, it can also be seen that MNFC fibrils have a smaller diameter than the TMP fibers. In addition, contrary to TMP, the MNFC fibrils seem to be randomly oriented in the film structure. *Fig 1* and *Fig 2* are used as references to identify TMP and MNFC layers in the z-structured papers.

When the MNFC is added in the top position, the top side of the paper presents a dense structure (*Fig 3b*), quite similar to the 100% MNFC films. The 3D view (*Fig 3a*) reveals the bilayer paper structure, *i.e.* a thin, apparently dense, shiny layer of MNFC on the top of a thick TMP fiber layer. For the inclusion of MNFC at the middle position, the paper surface (*Fig 4b*) resembles the 100% TMP sheet as it is composed of pure TMP fibers, notwithstanding potential variation due to drainage differences. The tri-layer paper structure can be observed from the 3D view (*Fig 4a*), *i.e.* a thin shiny layer of MNFC is sandwiched between the two TMP layers. The MNFC layer is clearly visible in the *z*-structured paper structure due to the presence of the calcium carbonate in the initial MNFC suspensions. Indeed, calcium carbonate has a different attenuation coefficient from the cellulosic fibers (Rolland du Roscoat et al., 2012). Furthermore, the difference in dimension between the MNFC fibrils and the TMP fibers facilitates their distinction in the paper structure.

The paper cross section (*Fig 5*) indicates that MNFC fibers (fibrils cannot be identified here) do not penetrate the TMP bottom layer in both middle and top positions. However, it clearly forms a layer in the paper thickness. This image confirms qualitatively the creation of *z*-structured paper.

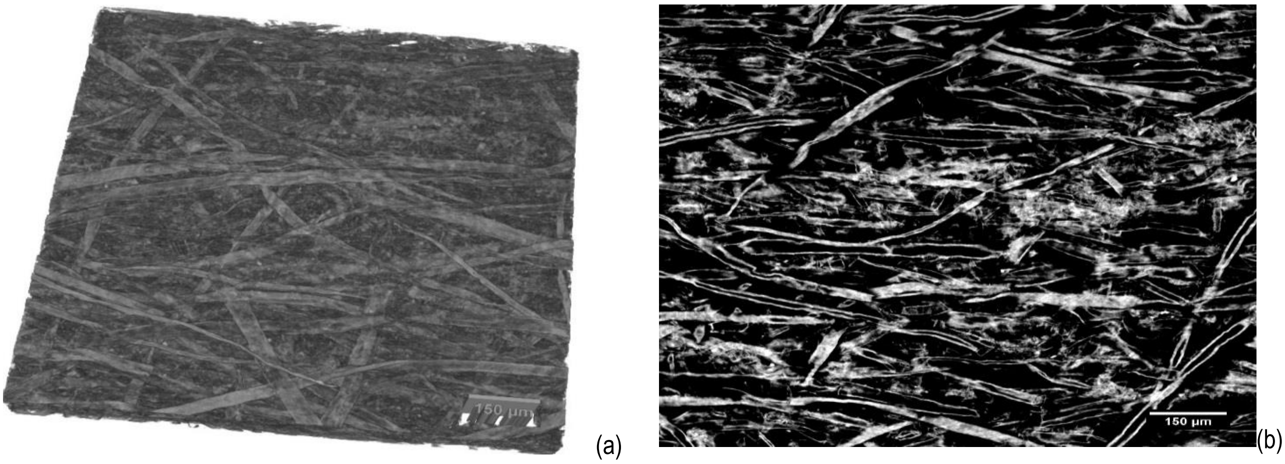

Fig 1 - 100% TMP sheet images: (a) 3D view (sample in the image size: 1 158 × 1 197 µm²), (b) internal paper structure (slice in the middle of the paper thickness).

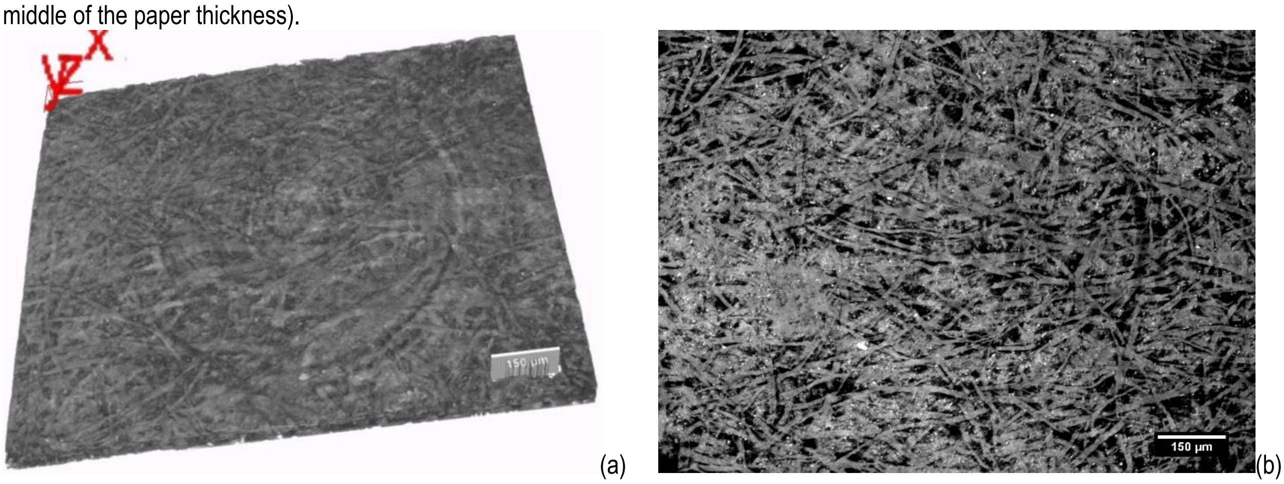

Fig 2 - 100% MNFC film images: (a) 3D view (sample in the image size: 1 310 × 1 002 µm²), (b) internal film structure (slice in the middle of the film thickness). The rings in the image are image capture artefacts.

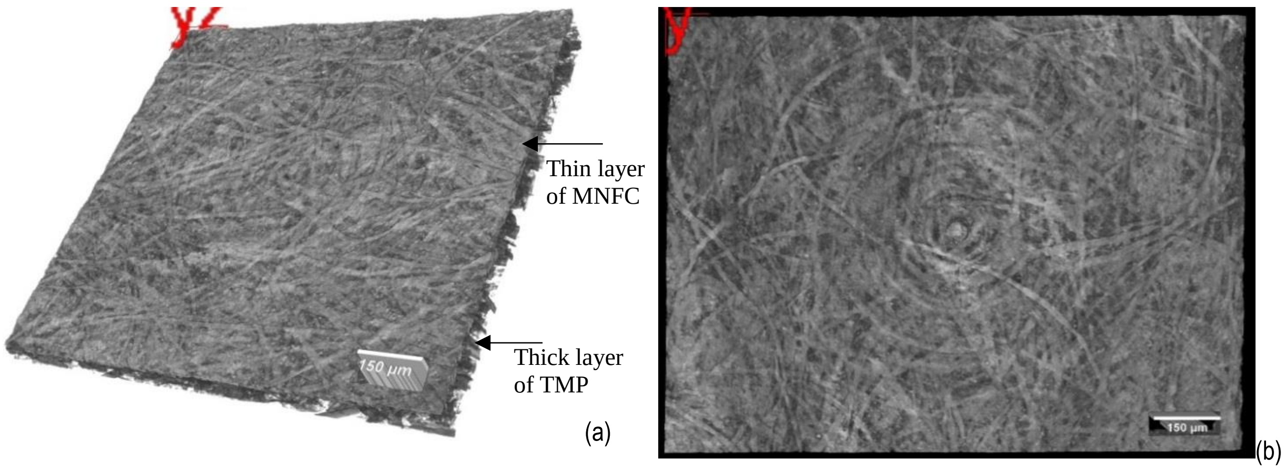

Fig 3 - 3D images of *z*-structured paper, 20 g.m^{-2} MNFC layer in the top position (a) 3D view (sample in the image size: 1 306 × 1 025 µm²), (b) top side view of the *z*-structured paper.

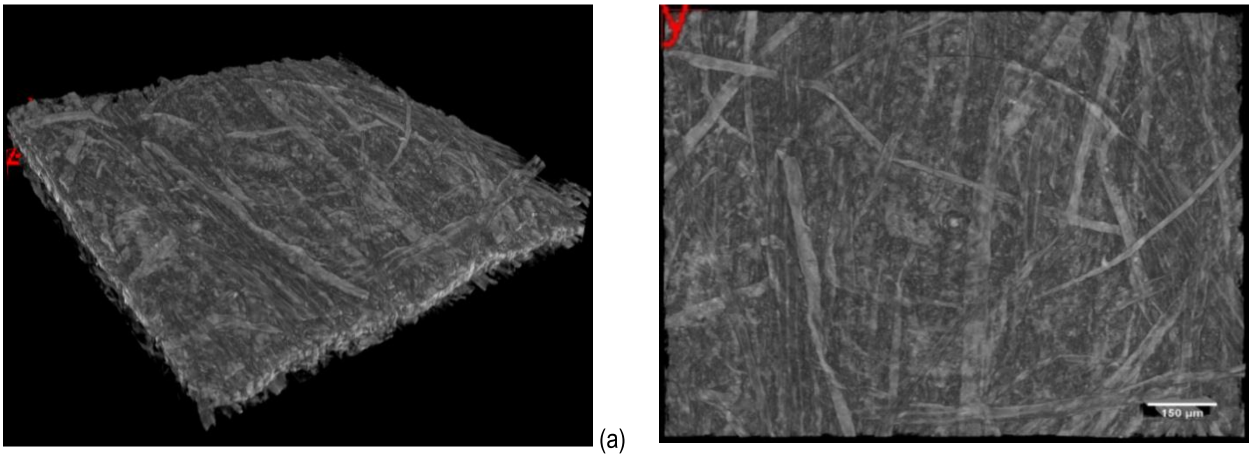

Fig 4 - 3D images of *z*-structured paper, 20 g.m^{-2} MNFC layer in the middle position (1 255 × 1 072 µm²) (a) sample 3D view (scale: 150 µm), (b) top side view of the *z*-structured paper.

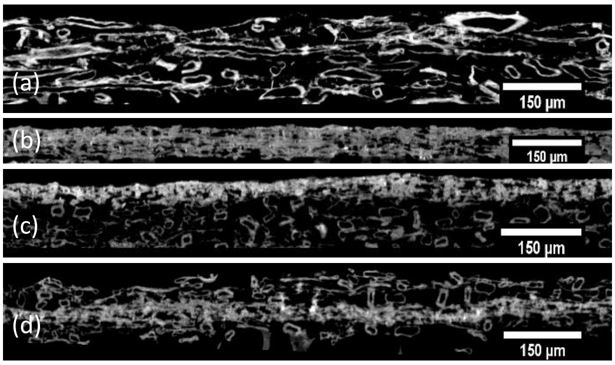

Fig 5- Images of the paper section, (a) 100 % TMP sheet, (b) 100% MNFC film, (c) 20 g.m^{-2} MNFC layer in the top position, (d) 20 g.m^{-2} MNFC layer in the middle position.

Porosity profile within the sheet thickness

From binary images, porosity was calculated as the ratio of the number of voxels in the pore phase compared to the voxel number in the total sample volume. Furthermore, porosity was calculated slice per slice, with a slice thickness of 0.65 µm, in the paper *z*-dimension, which allowed a plot to be made of the porosity profile in the direction of the paper thickness. A typical porosity profile for a fibrous monolayer paper reveals the presence of three porosity regions (Rolland du Roscoat et al., 2007). Two regions with a high porosity gradient represent the boundary top and bottom paper layers. The third region has almost a constant porosity, designated here as *bulk* porosity.

We normalized the values of each profile by the paper thickness, in order to obtain a common range of [0, 1]. For the next porosity profiles shown in *Fig 6-8*, the 0 value in the *x*-axis refers to the paper top side and the value of 1 refers to the bottom (or wire) side.

In *Fig 6*, a difference of 38% in the *bulk* porosity is observed between the 100% TMP sheet and the 100% MNFC film. TMP sheets have a measured *bulk* porosity around 76% and the MNFC film a mean *bulk* porosity around 38%. The paper porosity is increased due to the high porosity of the boundary layers. This difference confirms the capacity of MNFC to form a dense fibrillar network as proposed by Rodionova et al. (2012), when compared with TMP fibers.

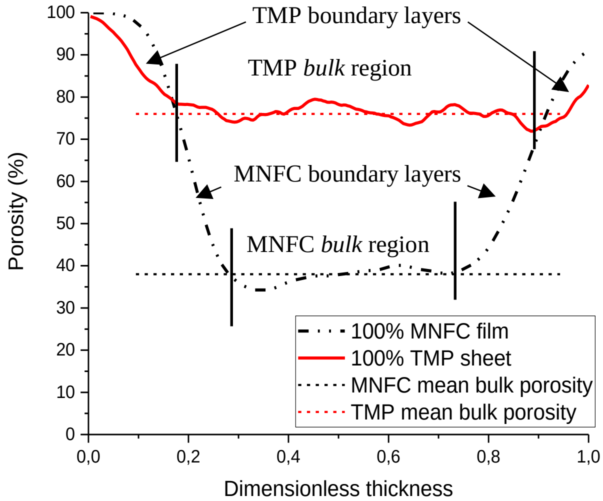

Fig 6 - Porosity profiles among the normalized thickness of the TMP and MNFC references.

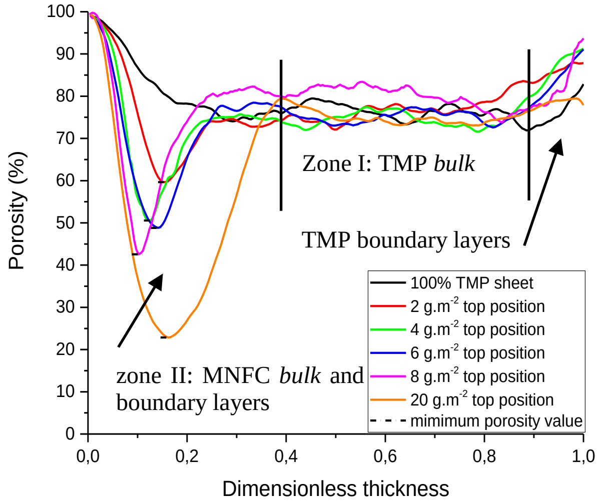

Fig 7 - Porosity profiles among the normalized thickness of the *z*-structured paper top position.

When the MNFC layer is added on the top of the TMP layer, the porosity profile (*Fig 7*) shows the *bulk* porosity region to be composed of two zones. A zone I, with a porosity of about 75% that corresponds to the TMP layer and a second zone II, on the top, with low porosity that corresponds to the MNFC layer. Although the minimum porosity ranges from about 60% (2 g.m^{-2}) to 43% (8 g.m^{-2}). The value corresponding to an addition of 20 g.m^{-2} (24%) is lower than the value for the pure MNFC film at 40 g.m^{-2} (38%). We surmise that there exists some level of imbrication or meshing between the TMP fines and the MNFC fibrous elements that leads to this lower porosity value.

For the addition of MNFC in the middle position (*Fig 8*), the porosity profile shows the presence of three zones in the *bulk* region that correspond to the three layers of the paper. Furthermore, the TMP layers exhibit different porosities, 73% and 78% for the top and bottom layers respectively, due to an important retention of the TMP fines in the top TMP layer compared to the bottom TMP layer. The MNFC layer acts as an additional drainage element retaining fines during the paper forming.

The porosity profiles indicate that the MNFC layer is formed at the targeted position. Furthermore, it does not seem to truly penetrate the TMP layer, although there is some level of interactions related to the fines in the TMP pulp. It should be recalled that the DSF just creates a wall of the fiber-water blend on a rotating cylinder, layer-by-layer, and subsequently the whole water-fiber slurry composite layer is drained through the wire in a single operation. The structure existing in the so-called water-fiber slurry wall is essentially retained in the dry sheet. These results confirm the feasibility of the *z*-structuring approach at the laboratory scale.

The MNFC layer thickness increases with its basis weight. This effect leads to a further decrease in the MNFC layer minimum porosity value (*Fig 9*) and to the increasing thickness of the MNFC region in the porosity profile. As seen for the top addition, the minimum value of porosity for the 20 g.m^{-2} addition of MNFC is lower than that of the pure MNFC sheet at 40 g.m^{-2}.

Accordingly, the minimum porosity values for both the top and middle addition positions were analyzed as a function of the MNFC layer basis weight addition. In *Fig 10*, the minimum porosity value is found to be inversely proportional to the MNFC basis weight. The inverse linear relationship from 2 to 20 g.m^{-2} addition, decreasing to 24%, is surprising, as one would have expected an asymptotic decrease towards the minimum porosity value of 38% obtained for the 40 g.m^{-2} pure MNFC film. Some interactions, imbrication or meshing between the MNFC fibrous material and the TMP may explain such an effect. The slight difference in lower porosity values between top and middle position may be explained by a better water evacuation from the MNFC layer structure during pressing. In fact, water extraction from the MNFC layer is easier when it is on the top position than in the middle position. The direct contact between the MNFC layer and the absorbent blotting paper used in pressing the DSF sheets obviously facilitates water extraction from the MNFC layer structure. In the middle position, the MNFC layer is somehow protected by the two TMP layers, and water must go through the TMP structures, clearly not as efficient as blotting paper, before being evacuated from the paper structure.

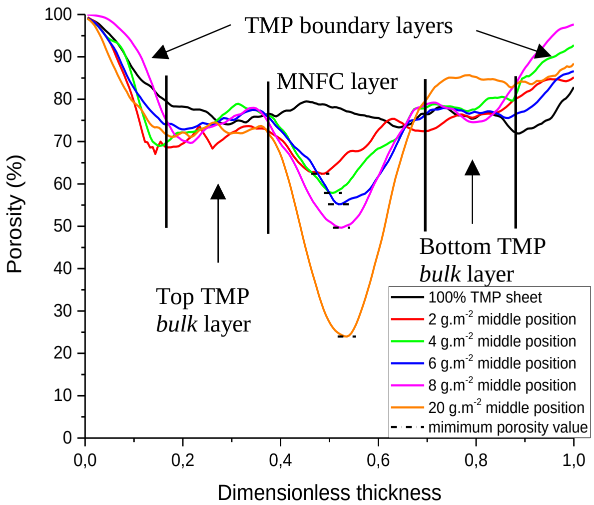

Fig 8 - Porosity profiles among the normalized thickness of the *z*-structured paper middle position.

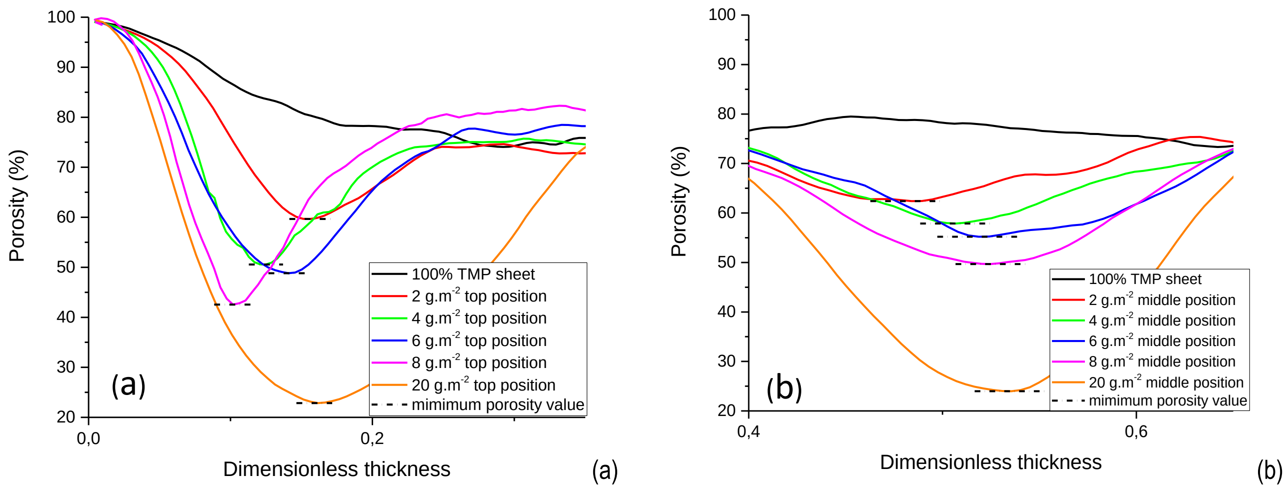

Fig 9 – MNFC layer porosity profile (MNFC zone) – top MNFC addition on left (a) and middle MNFC addition on right (b).

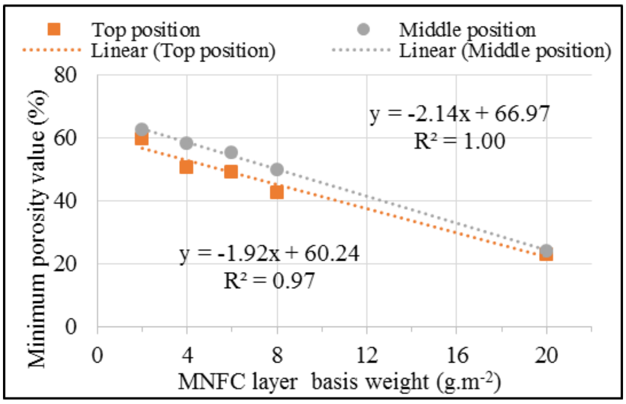

Fig 10 – MNFC layer minimum porosity variation as a function of the MNFC layer basis weight

Conclusions

The *z*-structuring hypothesis was tested using MNFC as a papermaking additive to create layered composite paper structures by design. MNFC was added as a layer ranging from 2 to 20 g.m^{-2} in two positions, namely on the top and in the middle of the thickness of the sheet, during the paper formation, to create a *z*-structured paper of a constant basis weight. Paper structures were then analyzed by synchrotron X-ray microtomography. Experimental results proved that; (i) the SμT technique is an efficient and well performing tool to identify the MNFC in the paper structure; (ii) the retention of the MNFC in the paper structure occurs within the targeted layer position. Porosity profiles through the paper thickness for a monolayer fibrous structure exhibited the presence of three porosity zones. Two zones with a high porosity gradient that represent the boundary sheet layers (top and bottom) and a third zone, that we called *bulk* porosity, with a relative constant porosity. When MNFC is added to the TMP pulp, *bulk* porosity is mainly affected. In contrast, in the case of layered composite forming addition, depending on the MNFC layer position, the *bulk* porosity is then composed of two or three different porosity zones that represent TMP and MNFC layers in the *z*-structured paper porosity profile.

Future work will focus on the macroscopic paper properties, *i.e*. mechanical and barrier properties, of the obtained structures, and how to elaborate such *z*-structured papers on a paper machine equipped with a curtain coating equipment.

Acknowledgements

The authors are grateful to Omya International A.G for financial support, especially Mr. Michel Schenker (Omya International AG) for providing the MNFC used in this study, and Prof. Patrick A.C. Gane (Aalto University and Omya International AG) and Dr. Cathy Ridgway (Omya International AG) for useful discussions during the course of the present work.

Literature

Aulin, C., Gällstedt, M. and Lindström, T. (2010): Oxygen and oil barrier properties of microfibrillated cellulose films and coatings, Cellulose, 17(3), 559-574.

Brodin, F. W., Gregersen, O. W. and Syverud, K. (2014): Cellulose nanofibrils: Challenges and possibilities as a paper additive or coating material—A review, Nord Pulp Pap Res J, 29(1), 156-166.

Eriksen, Ø., Syverud, K. and Gregersen, Ø. (2008): The use of microfibrillated cellulose produced from kraft pulp as strength enhancer in TMP paper, Nord Pulp Paper Res J, 23(3), 299-304.

González, I., Boufi, S., Pèlach, M. A., Alcalà, M., Vilaseca, F. and Mutjé, P. (2012): Nanofibrillated cellulose as paper additive in eucalyptus pulps, BioResources, 7(4), 5167-5180.

Lavoine, N., Desloges, I., Dufresne, A. and Bras, J. (2012): Microfibrillated cellulose - its barrier properties and applications in cellulosic materials: A review, Carbohydr Polym 90(2), 735-764.

Moore, M. J., Jabbari, E., Ritman, E. L., Lu, L., Currier, B. L., Windebank, A. J. and Yaszemski, M. J. (2004): Quantitative analysis of interconnectivity of porous biodegradable scaffolds with micro-computed tomography, J Biomed Mater Res Part A, 71A(2), 258-267.

Pyun, A., Bell, J. R., Won, K. H., Weon, B. M., Seol, S. K., Je, J. H. and Macosko, C. W. (2007): Synchrotron X-ray microtomography for 3D imaging of polymer blends, Macromolecules, 40(6), 2029-2035.

Rodionova, G., Eriksen, Ø. and Gregersen, Ø. (2012): TEMPO-oxidized cellulose nanofiber films: effect of surface morphology on water resistance, Cellulose, 19(4), 1115-1123.

Rolland du Roscoat, S., Bloch, J. F. and Caulet, P. (2012): A method to quantify the 3D microstructure of fibrous materials containing mineral fillers using X-ray microtomography: application to paper materials, J. Mater. Sci. 47(18), 6517-6521.

Rolland du Roscoat, S., Bloch, J. F. and Thibault, X. (2005): Synchrotron radiation microtomography applied to investigation of paper, J. Phys. D: Appl. Phys. 38(10A), A78-A84.

Rolland du Roscoat, S., Decain, M., Thibault, X., Geindreau, C. and Bloch, J. F. (2007): Estimation of microstructural properties from synchrotron X-ray microtomography and determination of the REV in paper materials, Acta Materialia, 55(8), 2841-2850.

Samuelsen, E. J., Helle, T., Houen, P. J., Gregersen, O. W. and Raven, C. (1999): Three-dimensional imaging of paper by use of Synchrotron X-ray Microtomography, Three-dimensional imaging of paper by use of Synchrotron X-ray Microtomography, pp. 307-312.

Siró, I. and Plackett, D. (2010): Microfibrillated cellulose and new nanocomposite materials: A review, Cellulose, 17(3), 459-494.

Syverud, K. and Stenius, P. (2008): Strength and barrier properties of MFC films, Cellulose, 16(1), 75-85.

Thibault, X., Bloch, J.-F. and Boller, E. (2002): Felt structure characterised by synchrotron microtomography, Appita J, 55(2), 145-148.

Manuscript received December 30, 2015
Accepted for publication March 20, 2016